Electromagnetic Modeling and Capacity Analysis of Rydberg Atom-Based MIMO System

Shuai S. A. Yuan, *Graduate Student Member, IEEE*, Xinyi Y. I. Xu, Jinpeng Yuan, Guoda Xie, Chongwen Huang, *Member, IEEE*, Xiaoming Chen, *Senior Member, IEEE*, Zhixiang Huang, *Senior Member, IEEE*, and Wei E. I. Sha, *Senior Member, IEEE*

***Abstract*—Rydberg atom-based antennas exploit the quantum properties of highly excited Rydberg atoms, providing unique advantages over classical antennas, such as high sensitivity, broad frequency range, and low intrinsic noise. Despite the increasing interests in their applications in antenna and communication engineering, some key properties, involving the lack of polarization multiplexing and isotropic reception without mutual coupling, remain unexplored in the analysis of Rydberg atom-based multiple-input–multiple-output (MIMO) communications. Generally, the design considerations for any antenna, even for atomic ones, can be extracted to factors, such as radiation pattern, efficiency, and polarization, allowing them to be seamlessly integrated into existing system models. In this letter, we extract the antenna properties from relevant quantum characteristics, enabling electromagnetic modeling and capacity analysis of Rydberg MIMO systems in both far-field and near-field scenarios. Focusing on spatial multiplexing performance under the same signal-to-noise level, our results indicate that Rydberg atom-based antenna arrays offer certain advantages over classical dipole-type arrays in single-polarization MIMO communications.**

***Index Terms*—Channel capacity, electromagnetics (EM), Green's function, multiple-input–multiple-output (MIMO) communications, Rydberg atomic antenna.**

I. Introduction

Wireless communications have evolved significantly over the years, transitioning from single-antenna systems to multiple-antenna configurations [1], then leading to massive [2] and even holographic antenna arrays [3]. The design of these advanced arrays enables the efficient and skillful utilization of spatial, angular, temporal, frequency, and polarization domains, thereby continuously improving communication performance. However, classical antennas are bounded by many intrinsic limitations, such as Chu's [4] gain-bandwidth limit and Hannan's [5] efficiency limit, which significantly constrain the potential performance enhancements of current communication systems.

Since it is challenging to overcome these classical limits through conventional physics, Rydberg atom-based receivers [6], [7], [8], [9], [10], [11], rooted in quantum physics, offer new possibilities by circumventing these restrictions. Rydberg atom-based antennas exhibit several attractive properties, including high sensitivity, broad frequency range, compact size, and low intrinsic noise, making them promising candidates for sensing [12], [13], [14], [15], [16], [17] and communication [7], [8], [18], [19]. Notably, a single-input multiple-output system has been developed [20], and direction-of-arrival (DOA) estimation has been achieved [21], paving the way for multiple-input–multiple-output (MIMO) applications. In addition, channel models and signal processing techniques have also been investigated for Rydberg MIMO communications [22], [23], [24], [25]. From an antenna engineering perspective, critical factors, such as radiation patterns, efficiency, and polarization, must be addressed, as they directly influence MIMO system performance. However, most existing research emphasizes hardware architectures or signal processing methods, with limited focus on extracting antenna properties specifically for MIMO purpose. Moreover, the electromagnetic (EM) modeling of such systems remains underdeveloped. A comprehensive approach that combines EM, quantum, and information theories is required to advance the understanding and application of Rydberg MIMO systems.

In this letter, we propose an EM model of Rydberg MIMO systems and perform capacity analysis at both far and near fields, leveraging the two key properties of isotropic reception and lack of polarization multiplexing. Our contributions can be summarized as follows.

1) The analysis of a two-level system $S_{1/2} \leftrightarrow P_{1/2}$ is presented to demonstrate why Rydberg systems are insensitive to polarization and direction in MIMO communications, and the distinction between polarization measurement and multiplexing communication is clarified.
2) The isotropic and polarization effects of Rydberg antenna are considered and integrated into EM-based models for both far-field and near-field communications. Capacity analyses are conducted for revealing the performance of Rydberg MIMO receiver at both far and near fields.

This work unifies the quantum properties of Rydberg antennas with the EM modeling of MIMO communication systems, offering valuable insights for the design of future Rydberg antenna arrays and communication systems.

Received 6 February 2025; accepted 5 March 2025. Date of publication 10 March 2025; date of current version 9 July 2025. This work was supported by the National Natural Science Foundation of China under Grant 61975177 and Grant U20A20164. *(Corresponding author: Wei E. I. Sha.)*

Shuai S. A. Yuan, Xinyi Y. I. Xu, Chongwen Huang, and Wei E. I. Sha are with the College of Information Science and Electronic Engineering, Zhejiang University, Hangzhou 310027, China (e-mail: weisha@zju.edu.cn).

Jinpeng Yuan is with the State Key Laboratory of Quantum Optics and Quantum Optics Devices, Institute of Laser Spectroscopy, Shanxi University, Taiyuan 030006, China.

Guoda Xie and Zhixiang Huang are with the Information Materials and Intelligent Sensing Laboratory of Anhui Province, Anhui University, Hefei 230039, China.

Xiaoming Chen is with the School of Information and Communications Engineering, Xi'an Jiaotong University, Xi'an 710049, China.

Digital Object Identifier 10.1109/LAWP.2025.3549313

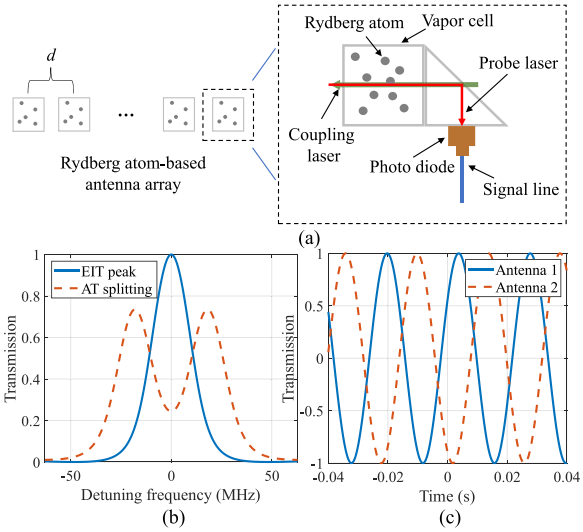

Fig. 1. Rydberg atom-based MIMO receivers. (a) Rydberg atom antenna array, the element spacing d is typically smaller than half-wavelength. (b) EIT and AT splitting in frequency domain analysis. (c) Time-domain signals from photo diodes for retrieving the amplitude and phase of incident wave.

II. Principles

A. Rydberg Atom-Based Antenna Array

Highly excited Rydberg atoms exhibit large transition dipole moments between neighboring Rydberg states, allowing them to resonate with EM waves across a broad frequency range[1] from MHz to THz [8], [9]. Fig. 1(a) illustrates the conceptual design of a Rydberg atom-based antenna array. By using coupling and probe lasers, the Rydberg atoms can detect incoming waves, effectively functioning as atomic antennas. In the frequency domain, electromagnetically induced transparency (EIT) can be established with two laser fields, enabling the Rydberg atoms to become transparent at certain frequencies. The Autler–Townes (AT) splitting effect, induced by microwave fields, facilitates precise field measurements and enables direct encoding and decoding of information [8], as shown in Fig. 1(b). Fig. 1(c) demonstrates how amplitude and phase information can be directly retrieved from photo diodes in time-domain measurements, typically using the superheterodyne technique with a local oscillator [21], [26]. Fig. 1(b) is generated using the fast algorithm for simulating the Rydberg response developed in our previous work [27], while Fig. 1(c) presents our experimental results for DOA estimation. In addition, because the atomic vapor is typically enclosed in glass, which has minimal scattering of EM waves, mutual coupling between atomic antennas is nearly negligible [28].

B. Antenna Radiation Pattern and Polarization

Intuitively, the Rydberg atoms are conducting stochastic motions in the vapor with no fixed dipole axis, making the receiver insensitive to electric field direction after averaging. To further illustrate this, we consider a system comprising two Rydberg energy levels, $S_{1/2}$ and $P_{1/2}$, each with two sublevels, $m_j = 1/2$ and $-1/2$. The Hamiltonian for the wave-atom interaction can be constructed based on this system.

[1] While the bandwidth of a single transition is typically narrow, on the order of kHz to MHz, it can be expanded by utilizing multiple transitions.

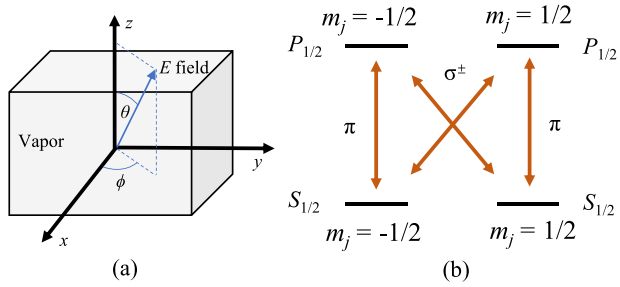

Fig. 2. Axis and level diagram for analyzing the effect of incoming wave direction and polarization. (a) Axis and relative angles, z-axis is set as the quantum axis, the angle between $+z$ and E-field is θ, the angle between $+x$ and the projection of E-field on xoy-plane is ϕ. (b) Level diagram with two Rydberg energy levels. The E-fields couple each sublevel of $S_{1/2}$ and $P_{1/2}$ through $\sigma^{\pm}$ or π transition, dependent on the wave polarization and direction.

According to the transition selection rules, the EM field couples these sublevels through π and $\sigma^{\pm}$ transitions with $\Delta m_j = 0$ and ± 1. The strength of the individual transitions depends on the orientation of the microwave field's polarization. The axis of this quantum system and the energy levels are depicted in Fig. 2. When the electric field E is along the z-axis, the Hamiltonian of this system can be represented by a matrix

$$\hat{H} = \frac{1}{2}\begin{pmatrix} 0 & 0 & -\Omega & 0 \\ 0 & 0 & 0 & \Omega \\ -\Omega^* & 0 & 0 & 0 \\ 0 & \Omega^* & 0 & 0 \end{pmatrix} \tag{1}$$

where the Ω is Rabi frequency, and the entries represent the interactions between the basis states $\left|S_{1/2}, -\frac{1}{2}\right\rangle$, $\left|S_{1/2}, \frac{1}{2}\right\rangle$, $\left|P_{1/2}, -\frac{1}{2}\right\rangle$, $\left|P_{1/2}, \frac{1}{2}\right\rangle$. As depicted in Fig. 2(b), only the π transition will appear between $S_{1/2}$ and $P_{1/2}$ with the same m_j. With arbitrary rotation of field direction and polarization, the angles between the axis and E can be denoted by θ and ϕ in Fig. 2(a). The contribution of E along z-axis accounts for the π transition, and the contribution along xoy plane accounts for the $\sigma^{\pm}$ transition with a phase shift $\exp(j\phi)$. Therefore, the Hamiltonian after arbitrary rotation of E field becomes

$$\hat{H}^{(\theta,\phi)} = \frac{1}{2}\times \begin{pmatrix} 0 & 0 & -\Omega\cos\theta & \Omega\sin\theta e^{-j\phi} \\ 0 & 0 & \Omega\sin\theta e^{j\phi} & \Omega\cos\theta \\ -\Omega^*\cos\theta & \Omega^*\sin\theta e^{-j\phi} & 0 & 0 \\ \Omega^*\sin\theta e^{j\phi} & \Omega^*\cos\theta & 0 & 0 \end{pmatrix}. \tag{2}$$

Solving the eigenvalues of (1) and (2), it can be found that they have the same eigenvalues $\pm\Omega/2$. Therefore, the direction of the electric field, and consequently the incoming wave direction and polarization, do not influence the Hamiltonian of this system. This process establishes the mapping from quantum properties to antenna characteristics, demonstrating that the Rydberg antenna inherently exhibits an isotropic radiation pattern and is polarization-independent. The AT frequency splitting Δ_{AT}, which can be directly measured in experiments, is equal to the energy difference between two eigenvalues, i.e., $\Delta_{\text{AT}} = \Omega$. After

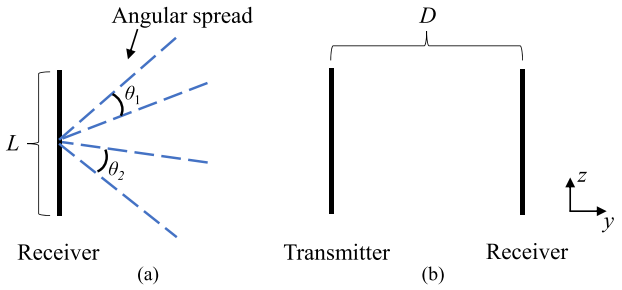

Fig. 3. Far-field and near-field communication scenarios, where the sizes of antenna arrays are fixed as $L \times L$, with $N \times N$ antennas uniformly distributed. L is fixed as 5 wavelengths in this article. (a) Far-field signals can be approximated as incoming plane waves inside certain angular spreads, and an isotropic scattering environment is considered here to match the isotropic pattern of Rydberg antenna. (b) At near field, the transmitting and receiving arrays are directly opposite at a distance D, with no scatterers between them.

that, we can obtain the electric field with

$$\Omega = \left| \frac{\mu E}{\hbar} \right| \tag{3}$$

where $\hbar$ is the Planck constant, μ is the transition dipole moment. Similar methods can be extended to more complex systems, and these principles have been experimentally verified [29], [30].

It is important to note that shifts or splittings of the field-modified spectroscopic lines depend on the amplitude of the EM field, while the relative strengths of these lines are determined by the orientation of the incident EM field polarization relative to the optical polarization [31]. Although this latter property can be employed for polarization measurement, current Rydberg atom systems rely on the shaping of spectroscopic lines for information transmission [8]. This suggests that polarization multiplexing cannot be used effectively, as the information would not be retrievable in such a configuration.

C. Antenna Efficiency

The configurations of the antenna arrays are plotted in Fig. 3. At far field, classical dipole-type antenna appears a cosine-shaped radiation pattern. Hannan's limit [5], [32] is employed to account for efficiency losses in dense array as $e = \pi S/\lambda^2$, where $S = (L/N)^2$ is the area of a single antenna element, λ is free-space wavelength. As the gain limit is a fundamental far-field bound, this efficiency limit concept should also hold for very dense atomic arrays. The efficiency formula for Rydberg antenna can be expressed as $e = 4\pi S/\lambda^2$, since the directivity of each electrically small Rydberg antenna is still 1 (isotropic), unlike the typical value of nearly 4 for dipole antenna. As atomic antennas lack the concept of impedance matching, the decrease in efficiency is likely due to insufficient interaction between the atoms and the field, potentially caused by smaller atom clusters in vapors, which requires further investigation. In this work, ideal efficiency is assumed for the Rydberg antennas, since the considered element spacing typically exceeds 0.3 wavelength.

III. EM-Based Modeling of Rydberg MIMO Systems

A. Far-Field Model

In the far-field scenario, the primary characteristics of Rydberg MIMO systems are the isotropic radiation pattern and the absence of mutual coupling. Consequently, far-field performance analysis can be readily conducted using existing ray-based methods [33], [34], with appropriate sampling of the radiation patterns. In this letter, we assume an isotropic scattering environment, which aligns with the characteristics of Rydberg antennas due to their isotropic patterns. The correlation coefficient between antennas at positions m and n can be determined with

$$r_{mn} = \frac{\iint E_m(\theta,\phi) E_n^*(\theta,\phi) \sin\theta \mathrm{d}\theta\mathrm{d}\phi}{\sqrt{\iint |E_m(\theta,\phi)|^2 \sin\theta \mathrm{d}\theta\mathrm{d}\phi} \sqrt{\iint |E_n(\theta,\phi)|^2 \sin\theta \mathrm{d}\theta\mathrm{d}\phi}} \tag{4}$$

where * denotes the conjugate operator, $E(\theta,\phi)$ is the far-field radiation pattern that directly determines the correlation, thus MIMO performance. More general forms can be easily included for dual polarizations, cross-polarization discrimination, and nonisotropic scattering environment [28], [33], [34]. After forming the correlation matrix $\mathbf{R}$, the channel matrix considering noise becomes $\mathbf{H} = (\mathbf{H}_w \mathbf{R}^{\frac{1}{2}})$, where the entries of $\mathbf{H}_w$ are independent identically distributed complex Gaussian random variables. The transmitting side is considered ideal appearing no correlations with ideal efficiency. Normalization of the channel matrix should be properly made for characterizing the realized gains of the antenna array, especially for dense array [35], [36]. Consequently, with power equally allocated, the ergodic capacity is given by

$$C = \mathcal{E}\left\{ \log_2 \left[\det\left(\mathbf{I} + \frac{\gamma}{N_t} \mathbf{H}\mathbf{H}^\dagger \right) \right] \right\} \tag{5}$$

where $\mathcal{E}$ denotes the ensemble average, $\mathbf{I}$ is the identity matrix, γ is the total signal-to-noise ratio (SNR), and N_t is the transmitting antenna number. Notice that the Rydberg antenna could exhibit significantly lower quantum noise compared to the thermal noise in traditional antennas [18], which generally allows for higher SNR. In this work, however, we assume an equal SNR level for both systems to facilitate a fair comparison of their spatial multiplexing performance.

B. Near-Field Model

For near-field model with no scatterers, the vector field should be considered, and we can use the free-space dyadic Green's function

$$\bar{\mathbf{G}}(\mathbf{r},\mathbf{r}') = \left(\bar{\mathbf{I}} + \frac{\nabla\nabla}{k^2} \right) g(\mathbf{r},\mathbf{r}') \tag{6}$$

where $\bar{\mathbf{I}}$ is the unit tensor, k denotes the wave number, $\mathbf{r}$ and $\mathbf{r}'$ are the positions of receivers and transmitters, and $g(\mathbf{r},\mathbf{r}')$ is the free-space scalar Green's function. The relation between source $\mathbf{J}(\mathbf{r}')$ and field $\mathbf{E}(\mathbf{r})$ can be written in matrix form and

$$\begin{bmatrix} E_x \\ E_y \\ E_z \end{bmatrix} = \begin{bmatrix} G_{xx} & G_{xy} & G_{xz} \\ G_{yx} & G_{yy} & G_{yz} \\ G_{zx} & G_{zy} & G_{zz} \end{bmatrix} \begin{bmatrix} J_x \\ J_y \\ J_z \end{bmatrix} \tag{7}$$

more explicit form of the Green's function can be found in the Appendix II of [36]. When considering full-polarizations at near field, we can form the channel matrix

$$\mathbf{H} = \begin{bmatrix} \mathbf{H}_{xx} & \mathbf{H}_{xy} & \mathbf{H}_{xz} \\ \mathbf{H}_{yx} & \mathbf{H}_{yy} & \mathbf{H}_{yz} \\ \mathbf{H}_{zx} & \mathbf{H}_{zy} & \mathbf{H}_{zz} \end{bmatrix}. \tag{8}$$

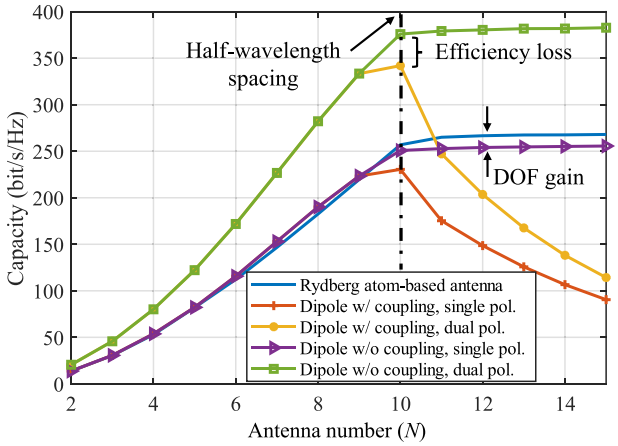

Fig. 4. Capacity comparison of MIMO systems build with Rydberg atom and dipole-type antennas at far field (SNR=10 dB). "w/o coupling" denotes the dipole array with ideal radiation efficiency.

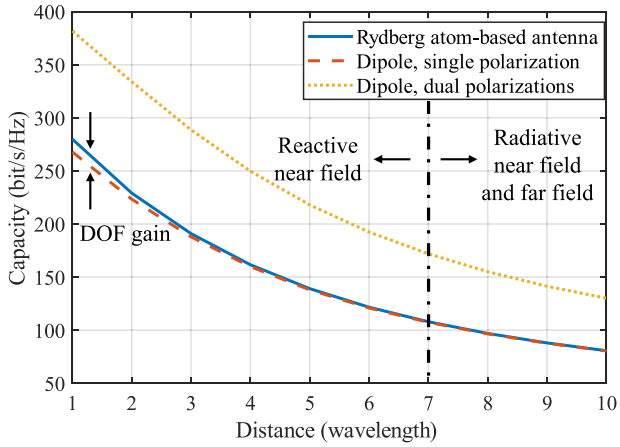

Fig. 5. Capacity comparison of MIMO systems build with Rydberg atom and dipole-type antennas at near field (SNR=10 dB).

For example, $h_{xx}(\mathbf{r},\mathbf{r}') = G_{xx}(\mathbf{r},\mathbf{r}')$ are the elements of channel matrix $\mathbf{H}_{xx}$ for the transmitters and receivers using x polarization [37]. The expressions for other polarizations follow similarly. Unlike classical systems fully described by (8), the Rydberg MIMO receiver does not differentiate between polarizations. Thus, the amplitude of received signal depends solely on the amplitude of total vector field $|E| = \sqrt{|E_x|^2 + |E_y|^2 + |E_z|^2}$, while the phase term is identical to that of a scalar Green's function, given by $\exp(-jk|\mathbf{r}-\mathbf{r}'|)$. Although, strictly speaking, only amplitude information can be observed [24], the phase can be directly retrieved from time-domain delays and is therefore considered explicitly known here for the purpose of spatial multiplexing analysis. In a more explicit form, the element for the channel matrix $\mathbf{H}_R$ is

$$h_R(\mathbf{r},\mathbf{r}') = \exp\left(-jk\left|\mathbf{r}-\mathbf{r}'\right|\right) \times \sqrt{\left|\sum_{i=x,y,z} G_{xi}\right|^2 + \left|\sum_{i=x,y,z} G_{yi}\right|^2 + \left|\sum_{i=x,y,z} G_{zi}\right|^2} \quad (9)$$

where the i denotes the polarizations used. Typically, a single polarization suffices, as no polarization gain is available. Compared to classical MIMO systems described by $\mathbf{y} = \mathbf{H}\mathbf{x}$, the model for Rydberg ones can be regarded as $\mathbf{y} = |\mathbf{H}_R\mathbf{x}|\mathbf{P}$, where the $|\cdot|$ here denotes entry-wise absolute value, $\mathbf{y}$ and $\mathbf{x}$ are the receiving and transmitting signals, $\mathbf{P}$ is a diagonal matrix containing the phase term $\exp(-jk|\mathbf{r}-\mathbf{r}'|)$ from the time-domain signal in photo diode. For conciseness, the influence of polarization is not explicitly denoted on $\mathbf{H}_R\mathbf{x}$, but is detailed in (9).

IV. Capacity Analysis

A. Far Field

The numerical results are shown in Fig. 4, where the capacity of classical MIMO system decreases after reaching half-wavelength spacing due to the efficiency loss caused by mutual coupling. While dual polarizations significantly increase capacity, a similar decline caused by mutual coupling at close antenna spacing is still observed. For Rydberg antennas with single polarization, even when compared to dipole antennas without mutual coupling, certain advantages are still evident, primarily due to their larger degree of freedom (DOF) in rich multipath environments [37]. In addition, although precoding is not applied in this case, the capacity trends remain similar, as they are primarily determined by the communication DOF. Moreover, the absence of mutual coupling makes Rydberg antenna a promising candidate for ultra-dense holographic arrays.

B. Near Field

At near field, we use (9) to construct the channel matrix for Rydberg MIMO system. For classical cases, $\mathbf{H}_{xx}$ from (8) is used for single polarization, while $[\mathbf{H}_{xx}, \mathbf{H}_{xy}; \mathbf{H}_{yx}, \mathbf{H}_{yy}]$ is used for dual polarizations. The element spacing is fixed as half wavelength for both transmitting and receiving sides, while the distance between them is changing. Compared to the channel matrix build with scalar Green's function [37], the main difference in the Rydberg MIMO system lies in the received amplitudes, which are calculated using the dyadic Green's function. The capacity results are shown in Fig. 5, where only minimal benefits are observed at very close distances for the Rydberg MIMO system. As the distance increases, approaching the radiative field region, the performance of both systems becomes nearly identical. Thus, while Rydberg atom-based receivers offer distinctive advantages in efficiency, size, and noise levels, their spatial multiplexing performance remains similar to that of classical antenna arrays.

V. Conclusion

This letter extracts key antenna properties from the quantum characteristics of Rydberg atom receivers, facilitating efficient analysis and seamless integration into existing MIMO system models. In general, the Rydberg antenna behaves like an isotropic scalar point receiver. The unique attributes of atomic antennas underscore their potential for communications in specific scenarios. For instance, Rydberg antennas offer orders of magnitude better sensitivity compared to traditional antennas. However, they also face challenges, such as high power requirements for lasers, and scalability limitations due to complex experimental setups. Overcoming these challenges will require advancements in both EM engineering and atomic physics. Further experimental and theoretical studies are crucial to fully unlocking their potential.

REFERENCES

[1] E. Telatar, "Capacity of multi-antenna Gaussian channels," *Eur. Trans. Telecommun.*, vol. 10, no. 6, pp. 585–595, 1999.

[2] E. G. Larsson, O. Edfors, F. Tufvesson, and T. L. Marzetta, "Massive MIMO for next generation wireless systems," *IEEE Commun. Mag.*, vol. 52, no. 2, pp. 186–195, Feb. 2014.

[3] C. Huang et al., "Holographic MIMO surfaces for 6G wireless networks: Opportunities, challenges, and trends," *IEEE Wireless Commun.*, vol. 27, no. 5, pp. 118–125, Oct. 2020.

[4] L. J. Chu, "Physical limitations of omni-directional antennas," *J. Appl. Phys.*, vol. 19, no. 12, pp. 1163–1175, 1948.

[5] P. Hannan, "The element-gain paradox for a phased-array antenna," *IEEE Trans. Antennas Propag.*, vol. AP-12, no. 4, pp. 423–433, Jul. 1964.

[6] Z. Ding et al., "A circularly-polarized omnidirectional Rydberg atomic sensor using characteristic mode analysis," *IEEE Trans. Antennas Propag.*, vol. 72, no. 12, pp. 9558–9563, Dec. 2024.

[7] J. Yuan, T. Jin, L. Xiao, S. Jia, and L. Wang, "A Rydberg atom-based receiver with amplitude modulation technique for the fifth-generation millimeter-wave wireless communication," *IEEE Antennas Wireless Propag. Lett.*, vol. 22, no. 10, pp. 2580–2584, Oct. 2023.

[8] D. A. Anderson, R. E. Sapiro, and G. Raithel, "An atomic receiver for AM and FM radio communication," *IEEE Trans. Antennas Propag.*, vol. 69, no. 5, pp. 2455–2462, May 2020.

[9] C. Holloway et al., "A multiple-band Rydberg atom-based receiver: AM/FM stereo reception," *IEEE Antennas Propag. Mag.*, vol. 63, no. 3, pp. 63–76, Jun. 2021.

[10] C. L. Holloway, M. T. Simons, J. A. Gordon, and D. Novotny, "Detecting and receiving phase-modulated signals with a Rydberg atom-based receiver," *IEEE Antennas Wireless Propag. Lett.*, vol. 18, no. 9, pp. 1853–1857, Sep. 2019.

[11] D. H. Meyer, K. C. Cox, F. K. Fatemi, and P. D. Kunz, "Digital communication with Rydberg atoms and amplitude-modulated microwave fields," *Appl. Phys. Lett.*, vol. 112, no. 21, 2018, Art. no. 211108.

[12] D. A. Anderson, R. E. Sapiro, and G. Raithel, "A self-calibrated SI-traceable Rydberg atom-based radio frequency electric field probe and measurement instrument," *IEEE Trans. Antennas Propag.*, vol. 69, no. 9, pp. 5931–5941, Sep. 2021.

[13] M. Jing et al., "Atomic superheterodyne receiver based on microwave-dressed Rydberg spectroscopy," *Nature Phys.*, vol. 16, no. 9, pp. 911–915, 2020.

[14] B. Liu et al., "Electric field measurement and application based on Rydberg atoms," *EMScience*, vol. 1, no. 2, pp. 1–16, 2023.

[15] J. Yuan et al., "Quantum sensing of microwave electric fields based on Rydberg atoms," *Rep. Prog. Phys.*, vol. 86, no. 10, 2023, Art. no. 106001.

[16] D. A. Anderson, E. G. Paradis, and G. Raithel, "A vapor-cell atomic sensor for radio-frequency field detection using a polarization-selective field enhancement resonator," *Appl. Phys. Lett.*, vol. 113, no. 7, 2018, Art. no. 073501.

[17] F. Zhang et al., "Quantum wireless sensing: Principle, design and implementation," in *Proc. 29th Annu. Int. Conf. Mobile Comput. Netw.*, 2023, pp. 1–15.

[18] C. T. Fancher, D. R. Scherer, M. C. S. John, and B. L. S. Marlow, "Rydberg atom electric field sensors for communications and sensing," *IEEE Trans. Quantum Eng.*, vol. 2, 2021, Art. no. 3501313.

[19] S. Mikki, "On the directivity of radiating quantum electromagnetic systems," *EMScience*, vol. 2, no. 3, pp. 1–19, 2024.

[20] J. S. Otto, M. K. Hunter, N. Kjærgaard, and A. B. Deb, "Data capacity scaling of a distributed Rydberg atomic receiver array," *J. Appl. Phys.*, vol. 129, no. 15, 2021, Art. no. 154503.

[21] A. K. Robinson, N. Prajapati, D. Senic, M. T. Simons, and C. L. Holloway, "Determining the angle-of-arrival of a radio-frequency source with a Rydberg atom-based sensor," *Appl. Phys. Lett.*, vol. 118, no. 11, 2021, Art. no. 114001.

[22] T. Gong et al., "Rydberg atomic quantum receivers for classical wireless communication and sensing," 2024, *arXiv:2409.14501*.

[23] T. Gong et al., "Rydberg atomic quantum receivers for classical wireless communications and sensing: Their models and performance," 2024, *arXiv:2412.05554*.

[24] M. Cui, Q. Zeng, and K. Huang, "IQ-aware precoding for atomic MIMO receivers," 2024, *arXiv:2408.14366*.

[25] M. Cui, Q. Zeng, and K. Huang, "Towards atomic MIMO receivers," *IEEE J. Sel. Areas Commun.*, vol. 43, no. 3, pp. 659–673, 2025, doi: 10.1109/JSAC.2025.3531528.

[26] M. T. Simons, A. H. Haddab, J. A. Gordon, and C. L. Holloway, "A Rydberg atom-based mixer: Measuring the phase of a radio frequency wave," *Appl. Phys. Lett.*, vol. 114, no. 11, 2019, Art. no. 114101.

[27] X. Y. I. Xu et al., "Fast simulation for interacting four-level Rydberg atoms: Electromagnetically induced transparency and Autler-Townes splitting," *Opt. Exp.*, vol. 32, no. 12, pp. 21755–21766, 2024.

[28] X. Chen, S. Zhang, and Q. Li, "A review of mutual coupling in MIMO systems," *IEEE Access*, vol. 6, pp. 24706–24719, 2018.

[29] M. Cloutman, M. Chilcott, A. Elliott, J. S. Otto, A. B. Deb, and N. Kjærgaard, "Polarization-insensitive microwave electrometry using Rydberg atoms," *Phys. Rev. Appl.*, vol. 21, no. 4, 2024, Art. no. 044025.

[30] S. Yuan, M. Jing, H. Zhang, L. Zhang, L. Xiao, and S. Jia, "Isotropic antenna based on Rydberg atoms," *Opt. Exp.*, vol. 32, no. 5, pp. 8379–8388, 2024.

[31] J. Sedlacek, A. Schwettmann, H. Kübler, and J. Shaffer, "Atom-based vector microwave electrometry using rubidium Rydberg atoms in a vapor cell," *Phys. Rev. Lett.*, vol. 111, no. 6, 2013, Art. no. 063001.

[32] S. S. A. Yuan, X. Chen, C. Huang, and W. E. I. Sha, "Effects of mutual coupling on degree of freedom and antenna efficiency in holographic MIMO communications," *IEEE Open J. Antennas Propag.*, vol. 4, pp. 237–244, 2023.

[33] X. Chen, P.-S. Kildal, J. Carlsson, and J. Yang, "MRC diversity and MIMO capacity evaluations of multi-port antennas using reverberation chamber and anechoic chamber," *IEEE Trans. Antennas Propag.*, vol. 61, no. 2, pp. 917–926, Feb. 2013.

[34] S. S. A. Yuan et al., "Breaking the degrees-of-freedom limit of holographic MIMO communications: A 3-D antenna array topology," *IEEE Trans. Veh. Technol.*, vol. 73, no. 8, pp. 11276–11288, Aug. 2024.

[35] S. Loyka and G. Levin, "On physically-based normalization of MIMO channel matrices," *IEEE Trans. Wireless Commun.*, vol. 8, no. 3, pp. 1107–1112, Mar. 2009.

[36] S. S. A. Yuan, L. Wei, X. Chen, C. Huang, and W. E. I. Sha, "Electromagnetic normalization of channel matrix for holographic MIMO communications," *IEEE Trans. Wirel. Commun.*, 2025, doi: 10.1109/TWC.2025.3543585.

[37] S. S. A. Yuan, Z. He, X. Chen, C. Huang, and W. E. I. Sha, "Electromagnetic effective degree of freedom of an MIMO system in free space," *IEEE Antennas Wireless Propag. Lett.*, vol. 21, no. 3, pp. 446–450, Mar. 2022.